# Monitoring of the 2018 Kilauea's eruption in the lower East Rift Zone using multi-temporal PALSAR-2 imagery

Wen Liu
*Graduated School of Engneering*
*Chiba University*
Chiba, Japan
wen.liu@chiba-u.jp

Fumio Yamazaki
*National Research Institute for Earth Science and Disaster Resilience*
Tsukuba, Japan
fumio.yamazaki@bosai.go.jp

***Abstract*— A large eruption occurred in Kilauea volcano's East Rift Zone (ERZ) on the island of Hawaii, U.S.A., from May 3 to September 4, 2018. Twenty-four fissures erupted lava near Leilani Estates and destroyed more than 700 houses. In this study, four pre-event and six co-event ALOS-2 PALSAR-2 images acquired from two neighboring ascending paths were applied to monitor the surface deformation and the expansion of lava flows on the ERZ. The deformation was estimated by the differential interferometric analysis. During the eruption, both Halemaʻumaʻu Crater and Puʻu ʻOʻo Crater went away from the PALSAR-2 sensor, whereas the Leilani Estates moved close to the sensor direction. The obtained movements were verified by comparing with GPS records. The lava flows from the Leilani Estates to the Pacific Ocean were detected by low backscattering in the intensity images. Finally, multi-temporal maps of the lava flows were created and compared with the maps published by U. S. Geological Survey.**

***Keywords—deformation, lava flows, interferometric analysis, thermal images, backscatter intensity***

## I. INTRODUCTION

Kilauea volcano is an active shield volcano in the island of Hawaii, U.S.A. It erupted continuously from 1983, causing significant damages. After a Mw 5.0 earthquake on May 3, 2018, ground cracks opened in the Leilani Estates and began to spew lava. By May 27, a total of 24 fissures had erupted lave near Leilani Estate and Lanipuna Gardens subdivisions. Approximately 2,000 residents were evacuated and 700 houses were destroyed. The volcano explosively erupted at the summit in Halemaʻumaʻu Crater on May 17, creating a plume of ash 30,000 feet into the air. At least two of lava flows reached the Pacific Ocean on May 9. By August 7, about 3.5 km2 of new land had been created in the ocean. Lava also entered the Puʻu Kapoho crater and evaporated the 400-year old Green Lake inside the crater, the largest natural freshwater lake in Hawaii. The re-erupted fissure 8 began to subside on August 5 and completely finished on August 15. On December 5, 2018, the eruption that started in 1983 was declared to be over.

The eruptions in volcanoes are typically accompanied by numerous earthquakes, the release of magmatic gases and surface deformation. Systematic volcano monitoring can provide early warning of volcanic catastrophes and necessary information for the assessment of hazards. Monitoring seismic signals is one of the most commonly way to determine the status of volcanos [1]. U. S. Geological Survey (USGS) Volcano Hazards Program set 69 seismometers, 72 GPS observation stations and 19 tiltmeters in the island of Hawaii [2]. Satellite images are also effective tools to continuously monitor volcanic activities. Multi-information could be obtained through the use of specific sensors on satellites [3, 4]. Furtney et al. [5] created two global databases of volcanic activities using synthetic aperture radar (SAR), thermal infrared images (TIR), and ultraviolet (UV) spectroscopy. Poland [6] measured the lava effusion of Kilauea volcano during 2011 to 2013 by calculating the differences in topography using the temporal digital elevation model. For the 2018 eruption event, USGS published the daily maps of fissure and lava flows from May 4 to August 14, 2018 [2], which were created from field surveys and thermal images.

In this study, four pre-event and six co-event ALOS-2 PALSAR-2 images obtained in the two neighboring ascending paths are used to monitor the 2018 eruption event. The involved deformation on Kilauea volcano's East Rift Zone (ERZ) is estimated by the differential interferometric analysis (DInSAR). Then the trails of lava flows are detected using the intensity images. Finally, the temporal lave maps are created and compared with the lave map by USGS.

## II. STUDY AREA AND PALSAR-2 DATA

The study area focused on Kilauea volcano's East Rift Zone (ERZ) including Halemaʻumaʻu Crater, Puʻu ʻOʻo Crater and Puna district, as shown in **Fig. 1**. The coverages of the four pre-event and six co-event ALOS-2 PALSAR-2 images are shown in **Fig. 1**, and their acquisition conditions are shown in **Table I**. All the images were taken in the path 89. The west path of the Beam No. U2-6 was acquired in the StripMap mode-1 using single HH polarization, whereas the east path of the Beam No. F2-6 was acquired in the StripMap mode-3 with HH and HV polarizations. The images were provided by complex data with the processing level 1.1.

The interferometric analysis and the pre-processing for the intensity images were carried out using ENVI SARscape software. After the multi-look compression (2 looks in each direction), the intensity images were geo-coded into a World Geodetic System (WGS) 84 reference ellipsoid by applying a 30-m SRTM digital elevation model (DEM). The pre- and co-event SAR images taken in the same path were registered by the cross-correlation method. The re-sampling pixel size was 5 m for the images in the west path and 10 m for the images in the east path. A radiometric calibration was conducted to transform the amplitude information into the backscattering coefficient ($\sigma 0$) [7].

A mosaic color composite of the geo-coded backscatter coefficient images after the pre-processing step is shown in **Fig. 2(a)**. The close-up of Halemaʻumaʻu Crater and Puʻu ʻOʻo Crater are shown in **Fig. 2(b)**. The color composite was

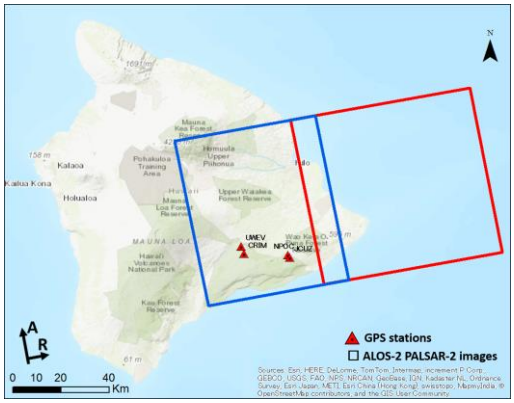


Fig. 1. Study area on Kilauea volcano's East Rift Zone (ERZ) in the island of Hawaii, U.S.A and the coverages of ALOS-2 PALSAR-2 images.

TABLE I. ACQUISITION CONDITIONS OF THE PALSAR-2 IMAGES

| Beam No. | U2-6 | F2-6 |
|---|---|---|
| **Pre-event** | 2015/04/28<br>2017/12/18 | 2018/01/30<br>2018/02/27 |
| **Co-event** | 2018/06/05 | 2018/05/08<br>2018/05/22<br>2018/06/19<br>2018/07/17<br>2018/08/14 |
| Polarization | HH | HH+HV |
| Heading [°] | 344 | 344 |
| Incident angle [°] | 32.4 | 36.3 |
| Resolution [m] (R×A) | 1.45×1.74 | 4.29×3.62 |

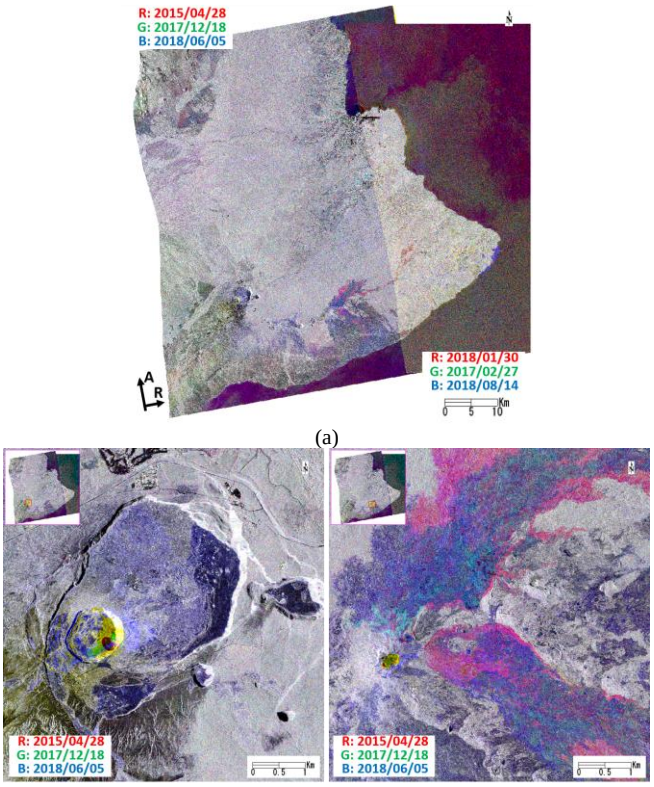


(a)

(b) Halemaʻumaʻu Crater (c) Puʻu ʻOʻo Crater

Fig. 2. Color comopsite of the backscatter intensity images: (a) the mosaic of two pairs including two pre-event and the last co-event images; (b-c) close-up of two signifiant changed craters.

consist of two pre-event and the last co-event images. The both craters showed yellow color, representing the decrease of backscatter during the eruption. According to the USGS [2], the crater floor of the cone of Puʻu ʻOʻo collapsed on April 30, 2018. The release of lava along the Lower ERZ led to significant drainage of lava away from Halemaʻumaʻu Crater, which caused inward slumping and collapsed around the crater from May 17. These collapses caused the decrease of backscatter in the co-event PALSAR-2 images. The blue color in the Kilauea Caldera represented the increase of backscatter, which was made by the accumulate volcanic ashes after the explosion at Halemaʻumaʻu Crater since May 9. The magenta color in the northeast and southeast of Puʻu ʻOʻo Crater represented the decrease of backscatter in 2017. It was due to the lava flowed from the vent "61g" since May 24, 2016. The blue color around Puʻu ʻOʻo Crater was considered as the increase of backscatter caused by the volcanic ashes.

## III. DEFORMATION ESTIMATION

The differential interferometric SAR analysis (DInSAR) was applied to the complex products of the slant-range PALSAR-2 data. For the west path, the image in 2017 was set as master. The baseline distance for the slave image in 2015 was 366 m, and that for the slave image in 2018 was 210 m. The 30-m SRTM DEM was introduced to remove elevation effects from the initial interferograms. Orbit fringes and noises were reduced by a Goldstein filter [8]. To remove the phase offset, 3 ground control points were selected manually in the stable area with high coherence and far away from the ERZ. Then the re-flattened fringes were unwrapped by the Minimum Cost Flow method [9] and transformed to the final line-of-sight (LOS) displacements. The obtained results from the two pairs are shown in **Fig. 3**. The positive values in the red color represent the movements toward to the sensor direction.

In the pre-event pair (2017 to 2015), the southwest part of Halemaʻumaʻu Crater moved 0.2 m close to the sensor direction. Since the master image was taken in 2017, it means this region moved far away from the sensor direction from 2015 to 2017. Besides this area, no significant movement was detected in the DInSAR result. In the pre- and co-event pair (2017 to 2018), the same area kept moving far away from the sensor direction. The displacements became significant, where the maximum value was 2.0 m. The long region around Puʻu ʻOʻo Crater also showed negative movements. The length of the far-away region was about 25 km. The largest movement in this area occurred in the east of the crater, which was 1.6 m in LOS. In the east region of this scene, positive movements were detected. The maximum value of the displacements was 1.0 m close to the sensor direction.

USGS Volcano Hazards Program set 24 GPS observation stations on the ERZ. The records of four stations were used to verify the estimated deformation of our DInSAR results. They located in the north and south of Halemaʻumaʻu Crater and Puʻu ʻOʻo Crater respectively, as shown in **Fig. 3**. A comparison of our results and the GPS records is shown in **Table II**. Excepting the station CRIM located in the south of Halemaʻumaʻu Crater, the other stations showed the southeast-forward movements and subsided. The station CRIM moved to the northwest and subsided. The three-dimension movements were read from the graphs of the two-

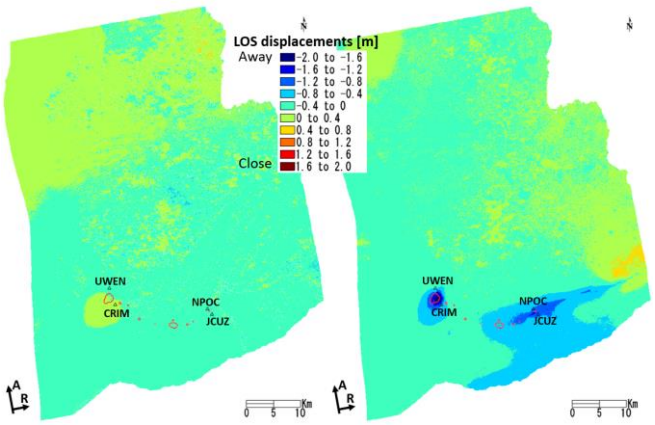


(a) 2017 to 2015 (b) 2017 to 2018

Fig. 3. Esitmated LOS displacements by the DInSAR analysis in the west path.

TABLE II. COMPARISON OF THE ESTIMATED DISPLACEMENTS AND THE RECORDS OF FOUR GPS OBSERVATION STATIONS

| Stations | DInSAR results [m] | | GPS records [m] | | | | Differences |
|---|---|---|---|---|---|---|---|
| | 2017 to 2015 | 2017 to 2018 | East | North | Up | LOS | [m] |
| UWEN | -0.04 | -0.38 | 0.43 | -0.53 | -0.34 | -0.43 | 0.05 |
| CRIM | 0.08 | -0.76 | -0.28 | 0.55 | -1.00 | -0.79 | 0.03 |
| NPOC | -0.14 | -0.87 | 0.44 | -0.54 | -0.86 | -0.87 | 0.01 |
| JCUZ | -0.16 | -0.95 | 0.59 | -0.65 | -0.85 | -0.92 | -0.02 |

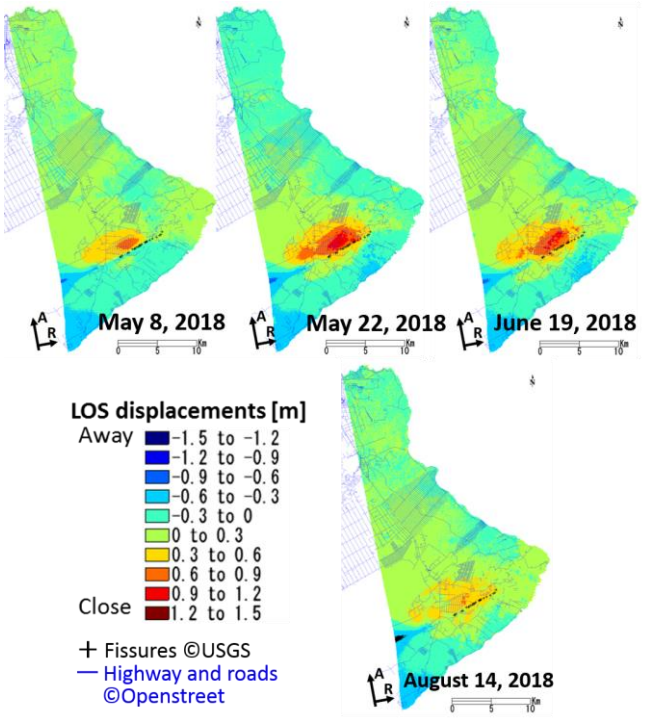


Fig. 4. Esitmated LOS displacements by the DInSAR analysis in the east path.

year GPS records [10] manually. Then they were transformed to the LOS displacements [11] according to the azimuth and incident angles. All the stations obtained negative values, moving away from the sensor direction. This trend matched with our DInSAR results. The maximum difference was only 5 cm, and the square root mean error for the four stations was 3 cm. Thus, the deformation obtained using the DInSAR analysis had a high accuracy.

For the east path, the image on February 27, 2018 was set as master. The baseline distances for the slave images were between 68 m to 210 m. The same InSAR processing was conducted. Different from the west path, no significant deformation was observed in the pre-event pair (January 3, 2018). Affected by the low coherence, the unwrapping processing failed in the pair on July 17. The estimated LOS displacements from the other four pairs are shown in **Fig. 4**. The close-forward movements could be confirmed in the northeastern of Leilani Estate. Comparing to the locations of fissures, the deformation occurred in the north side of the fissures' line. On May 8, about 2.7 km$^2$ area moved more than 0.6 m to the sensor direction. The maximum number of fringes was 7, representing 0.84 m displacement. On May 22, the deformation area became wider and the displacement was larger. 16.1 km$^2$ area moved more than 0.6 m close to the sensor direction, and 3.4 km$^2$ area with the larger displacements than 0.9 m. The maximum number of fringes was 12, representing 1.4 m displacements. By June 19, the significant deformation area reduced. About 11.2 km$^2$ moved more than 0.6 m close to the sensor direction. The maximum number of fringes was still 12. However, the area with larger displacements than 0.9 m reduced to 1.9 km$^2$ area. In the InSAR result on July 17, the fringe number decreased to 11. On August 14, only limited area showed larger displacement than 0.6 m. But we still could observe 11 fringes around Leilani Estate from the interferogram. It may be caused by errors in the unwrapping processing. The significantly changed surface led to the decrease of coherence. Then the fringes could not unwrap correctly. Comparing these obtained displacements, we could see the deformation had an increasing trend before May 22, and it became calm down later. Since there was no GPS station, it is difficult to verify the accuracy of the obtained results. Related to the results obtained in the west path, we considered the magma under Halemaʻumaʻu Crater and Puʻu ʻOʻo Crater moved along the ERZ to Leilani Estate, and erupted from the cracks.

## IV. EXTRACTION OF LAVA FLOWS

Coherence has been used to track lava flow on the ERZ of Kilauea volcano [12, 13]. We calculated the coherence between the images on February 27 and May 8, the one between the images on February 27 and August 14. The obtained coherences from Leilani Estate to the Pacific Ocean are shown in **Fig. 5** by the rainbow color. Before the volcano spewed out lava, most of the area showed higher coherence than 0.5, excepting several vegetated areas. In the second pair, the coherence decreased significantly in this area. Since both the affected and non-affected areas showed the decrease of coherence, it is difficult to extract the lava flow in this event by the coherence changes.

Color composites of the backscatter coefficients in the same area are shown in **Fig. 6**. Cyan and red colors could be confirmed from the fist combination before June 2018. It represented changes occurred between the image on May 8 and 22. Although lava had been erupted from May 5, the lava flow covered only 0.5 km$^2$ area [10]. Limited by the 10-m resolution and the long wavelength of L-band, the lava flows on May 8 could not be detected. In the second combination, cyan, red, yellow and magenta colors could be observed. It represented significant changes occurred during the acquired periods. The yellow and red regions along the coast were the new land created by the pouring lava.

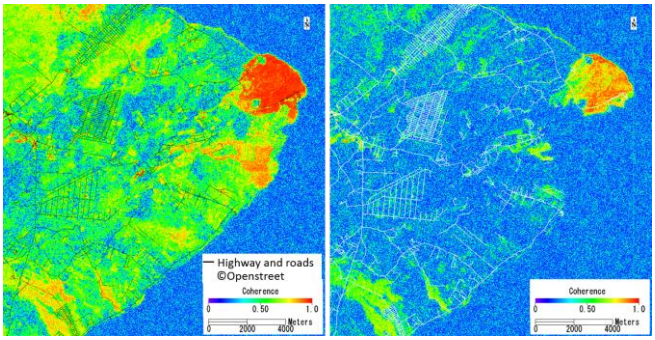


(a) (b)

Fig. 5. (a) Coherence between the SAR images on Feb. 27 and May 8, 2018. (b) Coherence between the SAR images on Feb. 27 and August 14, 2018.

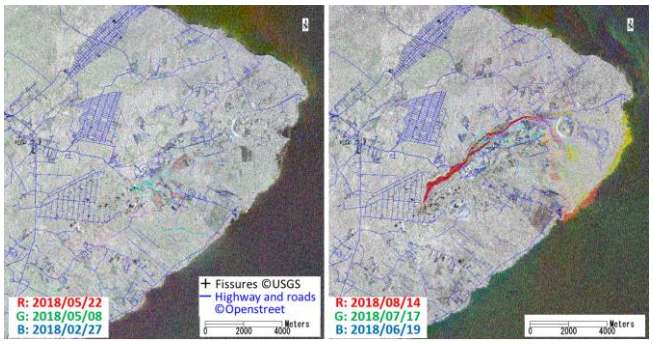


Fig. 6. Color composites of six temporal PALSAR-2 intensity images.

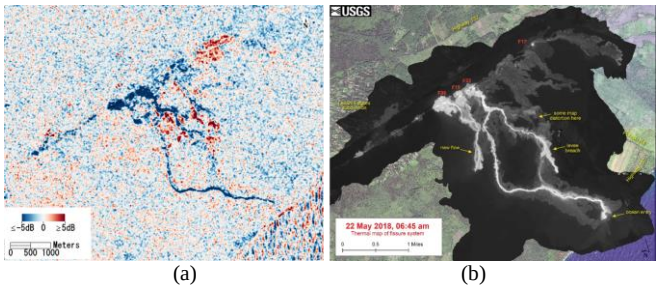


(a) (b)

Fig. 7. (a) Difference of the backscatter coeffciient by subtracting the image on May 22 from the image on Feburary 27, 2018. (b) A thermal map created by the USGS on May 22, 2018.

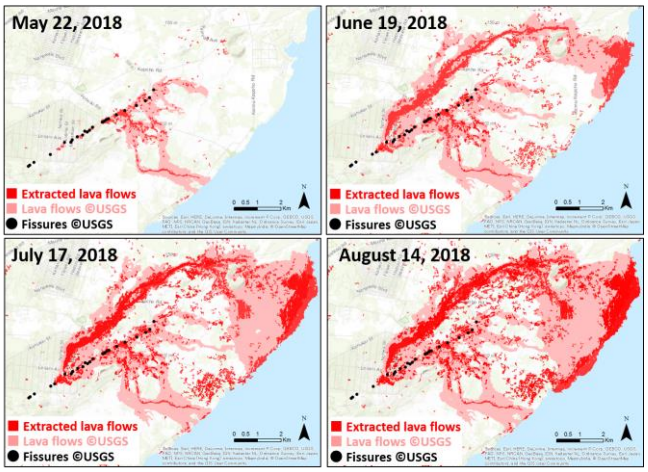


Fig. 8. Temporal maps of lava fows obtained from the PALSAR-2 images and estimated by the USGS.

To detect lava flows, the difference of backscatter coefficient was calculated by subtracting the master image in February from each slave images. The difference obtained between the image on May 22 and the master image is shown in **Fig. 7(a)**. In addition, a thermal map published by the USGS is shown in **Fig. 7(b)**. Since the thermal map was acquired at 06:45 and the PALSAR-2 image was acquired at 00:22, the lave flows in the thermal map were wider than those in the PALSAR-2 image. Comparing **Fig. 7(a)** and **(b)**, the lava flows with very high temperature showed the decrease of the backscatter coefficient, whereas some cooled down lava showed the increase of the backscatter coefficient. Then the area with the larger absolute difference than 3 dB was extracted as lava flows. To reduce noises, the extracted objects smaller than 30 pixels (3,000m$^2$) were removed from the results. In addition, sea masks were created for each slave image. The sea regions were extracted by the lower backscatter coefficient than -10 dB. The sea masks were applied to the differences to remove the noises due to the water waves. Comparing the sea mask on May 8 and August 14, the land expanded 3.5 km$^2$, which was the same number as the USGS's report [2].

The maps of the extracted lava flows are shown in **Fig. 8**. The lava flows published by the USGS are also shown in these maps. On May 22, 2018, 6.5-km$^2$ lava flows were reported by the USGS, whereas 1.9-km$^2$ area were detected from the SAR image. On June 19, 25.1-km$^2$ lava flows were reported by the USGS, whereas 10.8-km$^2$ area were detected from the SAR image. On July 17, 33.2-km$^2$ lava flows were reported by the USGS, whereas 16.0-km$^2$ area were detected from the SAR image. On August 14, 36.3-km$^2$ lava flows were reported by the USGS, whereas 19.9-km$^2$ area were detected from the SAR image. The PALSAR-2 images were good at extracting fluid lava flows with the high temperature but failed to detect the cool-down volcanic rocks. Thus, only half of the lava flows were extracted from the PALSAR-2 images. The area between two entering points were over-estimated as lava flows. This was caused by season changes in the agricultural fields. Most of the extracted area were within the lava flows reported by the USGS. Although, our results were underestimated, it still showed good potential to estimate the affected areas and is useful for the damage assessment.

## V. Conclusions

In this study, the surface deformation and the lava flows involved by the 2018 eruption of Kilauea volcano in the island of Hawaii, U. S. A., were detected using four pre-event and six co-event ALOS-2 PALSAR-2 images. By the DInSAR analysis, the far-away movements were observed around Halemaʻumaʻu Crater and Puʻu ʻOʻo Crater, whereas the forward movements were estimated in Leilani Estates. It is considered that the magma moved from the two craters to the fissures. The comparison of the obtained deformation and the records of four GPS stations was conducted. The InSAR results showed a high accuracy in the LOS displacements. Then the erupted lava flows were extracted by the temporal differences of backscatter coefficient. The fluid lava with high temperature could be identified by the low backscatter coefficient. The increase of backscatter coefficient was observed on same cool-down lava rocks. Comparing to the map obtained by the field surveys and the thermal images, the PALSAR intensity images could extract more than half of the affected regions. The 3.5-km$^2$ new land created by the pouring lave into the ocean was detected successfully from the temporal SAR intensity images. In the future, the

elevation would be considered to improve the extraction of the cool-down lava.

## ACKNOWLEDGMENT

The ALOS-2 PALSAR-2 data are owned by the Japan Aerospace Exploration Agency (JAXA) and were provided through the ALOS-2 research program (RA6, PI No. 3243). This work was partially supported by JST CREST Grant Number JPMJCR1411, Japan, and JSPS KAKENHI Grant Numbers 17H02066, Japan.

## REFERENCES

[1] E. T. Endo, T. Murray, "Real-time seismic amplitude measurement (RSAM): a volcano monitoring and prediction tool," Bulletin of Volcanology, vol. 53, issue 7, pp. 533-545, 1991.

[2] United States Geological Survey (USGS), "Volcano Hazards Program," 2018. https://volcanoes.usgs.gov/volcanoes/kilauea/

[3] C. Bignami, S. Corradini, L. Merucci, L., de Michele, D. Raucoules, S. Stramondo, J. Piedra, "Multi-sensor satellite monitoring of the 2011 Puyheue-Cordon Caulle Eruption," vol. 7, no. 7, 2014.

[4] M. E. Pritchard, M. Simons,"A satellite geodetic survey of large-scale deformation of volcanic centres in the central Andes," Nature, vol. 418, no. 6894, pp. 167–171, 2002.

[5] M. A. Furtney, M. E. Pritchard, J. Biggs, S. A. Carn, S. K. Ebmeier, J. A. Jay et al., "Synthesizing multi-sensor, multi-satellite, multi-decadal datasets for global volcano monitoring," Journal of Volcanology and Geothermal Research, vol. 365, pp. 38-56, 2018.

[6] M. P. Poland, "Time-averaged discharge rate of subaerial lavaat Kīlauea Volcano, Hawai'i, measuredfrom TanDEM-X interferometry: Implications for magma supplyand storage during 2011–2013," Journal of Geophysical Research: Solid Earth, vol. 119, pp. 5464-5481, 2014.

[7] Japan Aerospace Exploration Agency, "Calibration Result of ALOS-2/PALSAR-2 JAXA Standard Products," 2018. https://www.eorc.jaxa.jp/ALOS-2/en/calval/calval_index.htm

[8] R. M. Goldstein, C. L. Werner, "Radar intererogram filtering for geophysical application," Geophysical Research Letter, vo. 25, no. 21, pp. 4035-4038, 1998.

[9] M. Costantini, "A novel phase unwrapping mehod based on network programming," IEEE T. Geosci. Remote., vol. 36, no. 3, pp. 813-821, 1998.

[10] Hawaii Tracker, 2019. https://hawaii.jointracker.com/monitoring/2-year-gps

[11] W. Liu, F. Yamazaki, M. Matsuoka, T. Nonaka, T. Sasagawa, "Estimation of three-dimensional crustal movements in the 2011 Tohoku-oki, Japan earthquake from TerraSAR-X intensity images," Natural Hazards and Earth System Sciences, vol. 15, pp. 637-645, 2015.

[12] H. A. Zebker, P. Rosen, S. Hensley, P. J. Mouginis‐Mark, "Analysis of active lava flows on Kilauea volcano, Hawaii, using SIR‐C radar correlation measurements," Geology, vol. 24, pp. 495-498, 1996.

[13] H. R. Dietterich, M. P. Poland, D. A. Schmidt, K. V. Cashman, D. R. Sherrod, A. T. Espinosa, " Tracking lava flow emplacement on the east rift zone of Kīlauea, Hawai'i, with synthetic aperture radar coherence," Geochemistry, Geophysics, Geosystems, vol. 13, issue 5, 2012.